

Combined Hall-Sensor Calibration and MTPA Control for BLDC Motors with Large Stator Inductance

Ryan Edric Nashota
Mechanical Engineering
University of British Columbia
Vancouver, Canada
rnashota@student.ubc.ca

Mark Phung
Engineering Physics
University of British Columbia
Vancouver, Canada
marklong@student.ubc.ca

Juri Jatskevitch
Electrical and Computer Engineering
University of British Columbia
Vancouver, Canada
jurij@ece.ubc.ca

Abstract—Brushless DC (BLDC) motors are extensively utilized in industrial applications, yet they frequently encounter performance limitations due to Hall-sensor misalignment and significant stator inductance. These non-idealities manifest as torque ripple, acoustic noise, and a reduction in torque-per-ampere capability. This paper presents a unified control strategy that synergizes a lookup-table (LUT) based Hall-sensor calibration with a Maximum Torque Per Ampere (MTPA) Proportional-Integral (PI) controller. The proposed calibration routine employs an extrapolated averaging technique to rectify commutation intervals without introducing filter delays. Concurrently, the MTPA controller dynamically compensates for the current phase lag by adjusting the advance firing angle, thereby driving the average d-axis current to zero. Verification through detailed machine simulations confirms that the combined approach effectively restores balanced commutation and enhances torque generation efficiency compared to uncompensated baselines.

Index Terms—BLDC motor, Hall-sensor misalignment, MTPA, Lookup Table (LUT), Advance Angle Control.

I. INTRODUCTION

A. Background

Brushless DC (BLDC) motors are widely used in modern industries such as electric mobility, robotics, manufacturing, and industrial automation due to their high power density, good reliability and efficiency, superior torque-speed characteristics, simplicity, and low cost [3], [4]. Among various motor drive methods, Hall-sensor-controlled BLDC machines are commonly chosen for their ability to operate at a wide range of speeds and in applications where sensorless control may not be preferred [3], [4].

A BLDC motor consists of a permanent magnet synchronous machine (PMSM), which is electronically commutated by a voltage source inverter (VSI). A schematic diagram of a typical BLDC motor drive is shown in Fig. 1-1, where the VSI is controlled using three Hall sensors that detect the rotor position [5]. Each Hall sensor outputs a square wave signal with a value of 1 or 0, depending on the rotor position. To provide six evenly spaced readings, the three Hall sensors must be spaced apart by 120° [5]. In the 120° commutation scheme used in this work, each phase conducts for two-thirds of the electrical cycle [7]. In common operating mode

(COM), the VSI shifts its switching by 30° ahead of the Hall state transitions [8]. When stator inductance is negligible, the 30° shift aligns the fundamental component of the phase current with the phase back electromotive force (EMF), thus enabling maximum torque-per-ampere (MTPA) operation [8]. However, motors with significant stator inductance require dynamic adjustment of the advance firing angle to maintain MTPA operation.

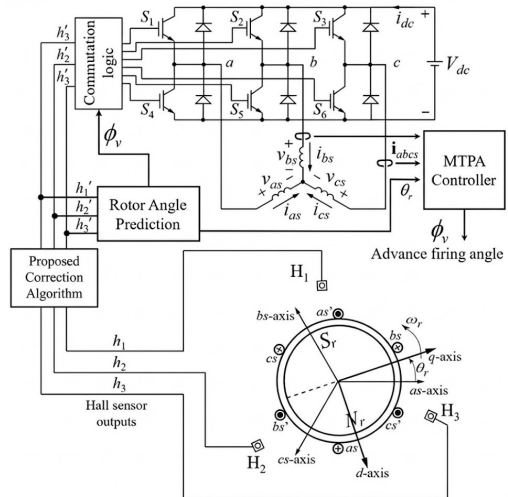


Fig. 1: Diagram for a Hall-sensor controlled BLDC motor driven by a VSI. The misaligned Hall sensors are passed through the proposed algorithm.

Furthermore, manufacturing imperfections cause the Hall sensors to deviate from their intended 120° spacing, resulting in asymmetric commutation timing as shown in Figure 4. This leads to imbalanced currents across phases, elevated torque oscillations, and overall degradation of motor performance [6]–[9]. Signal conditioning techniques, including moving average filters, have been applied to Hall sensor outputs [6], [9], yet these introduce timing delays that further compromise MTPA alignment. In motors with large winding inductance,

proportional-integral controllers have been developed to dynamically adjust the commutation advance angle [10]–[12]. However, these compensation strategies rely on accurate rotor position estimation, which becomes unreliable when the Hall sensors themselves are misaligned.

Thus to combat these problems, this paper builds upon previous work and presents a practical dual-strategy approach combining lookup table (LUT) calibration [2] with dynamic MTPA advance angle control [1] to simultaneously correct for Hall sensor positioning errors and compensate for inductance-related phase lag in 120° commutation mode. The proposed method is validated through simulation using MATLAB/Simulink on an industrial BLDC motor model exhibiting significant Hall misalignment and high winding time constant.

B. Modeling of the BLDC System

The BLDC motor will be modeled as a surface-mounted Permanent Magnet Synchronous Machine (PMSM). For this machine topology, the direct and quadrature axis inductances are equal, that is, $L_d = L_q = L_s$ [3], where L_s denotes the synchronous inductance, L_d the direct axis inductance and L_q the quadrature axis inductance. We will show later that this equality simplifies the analysis and is a defining characteristic of surface-mounted PMSMs.

The stator voltage equation in the stationary *abc* reference frame can be expressed as:

$$\mathbf{v}_{abc} = R_s \mathbf{i}_{abc} + L_s \frac{d}{dt} \mathbf{i}_{abc} + \mathbf{e}_{abc} \quad (1.1)$$

where \mathbf{v}_{abc} , \mathbf{i}_{abc} , and \mathbf{e}_{abc} are the phase voltage, current, and back-EMF vectors respectively, and R_s is the stator resistance.

While the *abc* frame provides a direct physical representation of the machine quantities, Maximum Torque Per Ampere (MTPA) control design is significantly simplified by converting to the synchronous rotating reference frame. To facilitate MTPA, we transform the system variables into the *dq* reference frame using the Park transformation matrix $\mathbf{K}_s^r(\theta_r)$:

$$\mathbf{K}_s^r(\theta_r) = \frac{2}{3} \begin{bmatrix} \cos(\theta_r) & \cos(\theta_r - \frac{2\pi}{3}) & \cos(\theta_r + \frac{2\pi}{3}) \\ \sin(\theta_r) & \sin(\theta_r - \frac{2\pi}{3}) & \sin(\theta_r + \frac{2\pi}{3}) \\ 1/2 & 1/2 & 1/2 \end{bmatrix} \quad (1.2)$$

where θ_r is the electrical rotor position. This transformation aligns the reference frame with the rotor flux, converting the time-varying *abc* quantities into constant or slowly varying *dq* quantities under steady-state operation.

Applying the Park transformation to (1.1), we obtain the dynamic equations in the *dq* frame:

$$v_q = R_s i_q + L_q \frac{di_q}{dt} + \omega_r L_d i_d + \omega_r \psi_m \quad (1.3)$$

$$v_d = R_s i_d + L_d \frac{di_d}{dt} - \omega_r L_q i_q \quad (1.4)$$

where ω_r is the electrical rotor speed, ψ_m is the permanent magnet flux linkage, and the coupling terms $\omega_r L_d i_d$ and $\omega_r L_q i_q$ represent the rotational back-EMF components in each axis.

The mechanical dynamics are governed by:

$$J \frac{d\omega_m}{dt} = T_e - T_L - B\omega_m \quad (1.5)$$

where J is the rotor inertia, ω_m is the mechanical rotor speed, T_L is the load torque, B is the viscous friction coefficient, and T_e is the electromagnetic torque. The electrical and mechanical speeds are related by $\omega_r = P\omega_m$, where P is the number of pole pairs.

By the principle of electromechanical energy conversion [3], the electromagnetic torque for a machine with P pole pairs is given by:

$$T_e = \frac{3P}{2} [\psi_m i_q + (L_d - L_q) i_d i_q] \quad (1.6)$$

By recognizing that for the surface-mounted PMSM, where $L_d = L_q = L_s$, the reluctance torque term $(L_d - L_q) i_d i_q$ vanishes, and the voltage equations also simplifies with $L_d = L_q = L_s$. Hence the torque equation reduces to:

$$T_e = \frac{3P}{2} \psi_m i_q \quad (1.7)$$

In the *dq* frame, we can clearly see how we can achieve Maximum Torque Per Ampere control. Notice from (1.7) that the *d*-axis current i_d does not contribute to the electromagnetic torque production. Instead, i_d only increases the stator current magnitude and consequently the copper losses, which scale with $I^2 R_s$ where $I = \sqrt{i_d^2 + i_q^2}$. To maximize torque efficiency and minimize losses per ampere, the optimal control strategy should maintain $i_d = 0$, thereby aligning all stator current with the torque-producing *q*-axis.

In the context of six-step commutation, the controller must regulate the commutation instants to maintain the time-averaged *d*-axis current magnitude close to zero while maximizing the *q*-axis current component [1], [7]. This ensures efficient operation and maximum torque output for a given current magnitude.

C. Inductive Phase Lag and Angle Compensation

In the ideal case where stator inductance is negligible, the voltage equations (1.3) and (1.4) simplify to their resistive forms:

$$v_q \approx R_s i_q + \omega_r \psi_m, \quad v_d \approx R_s i_d \quad (1.8)$$

In this case, the back-EMF components are

$$e_{qs} = \omega_r \psi_m, \quad e_{ds} = 0 \quad (1.9)$$

Note that this means when the current phase is aligned with the back-EMF, the current is purely *q*-axis and $i_d \approx 0$. Previous analysis has shown that advancing the commutation by 30° from the Hall sensor transition, results in fundamental current aligning with the *q*-axis [7], [8]. This results in $i_d \approx 0$ and achieves the MTPA condition.

However, for motors with non-negligible stator inductance, the inductive terms in (1.3) and (1.4) become significant. [3]. There will be commutation delay caused by the dynamic terms $L_s \frac{di_q}{dt}$ and $L_s \frac{di_d}{dt}$, which describes how the phase current

must transition from zero to its conducting value for each commutation.

Additionally, the rotational coupling terms $\omega_r L_s i_d$ in (1.3) and $\omega_r L_s i_q$ in (1.4) scale proportionally with rotor speed. At higher speeds, these terms become significant relative to the resistive drops, creating cross-axis voltage coupling that further delays the current response. The combined effect of both the transient and rotational inductive terms causes the fundamental component of the phase current to lag behind the back-EMF $e_{qs} = \omega_r \psi_m$ by an angle ϕ_v , as illustrated in Figure 2.

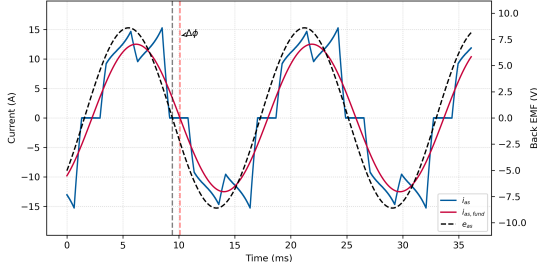


Fig. 2: Phase current fundamental component lags back-EMF due to stator inductance, causing angle ϕ_v that increases with rotor speed ω_r .

The consequence of this misalignment is a non-zero average d -axis current \bar{i}_d . Recall from (1.7) that only i_q contributes to electromagnetic torque. When the phase current lags the back-EMF, a portion of the stator current magnitude is directed along the d -axis, which does not produce torque but increases copper losses proportional to $i_d^2 R_s$. Therefore, for a given torque requirement, the motor must draw higher stator current, reducing the torque-per-ampere ratio defined as

$$TPA = \frac{T_e}{I_{rms}} = \frac{T_e}{\sqrt{i_d^2 + i_q^2}} \quad (1.10)$$

To recover MTPA operation and maximize (1.10), the commutation timing must be advanced by a compensation angle ϕ_v such that the effective firing angle becomes $\phi'_v = 30^\circ + \phi_v$. This compensation realigns the current with the back-EMF, forcing $\bar{i}_d \rightarrow 0$ and ensuring all stator current contributes to torque production. The required compensation angle ϕ_v is operating-point dependent, as it varies with speed ω_r , torque T_e , and DC bus voltage v_{dc} , necessitating a dynamic controller rather than a fixed offset [1], [7].

D. Hall Sensor Misalignment and Its Impact on MTPA Control Accuracy

Ideally, the three Hall sensors H_1 , H_2 , and H_3 should be positioned exactly 120° electrical apart to provide six equally-spaced rotor position estimates per electrical cycle. However, as illustrated in Figure 3, practical sensors deviate from ideal positions due to manufacturing tolerances.

These angular offsets creates distortion as visualized in Figure 4. Let Δt_n denote the time duration of the n -th switching interval. Ideally, all six intervals within one electrical

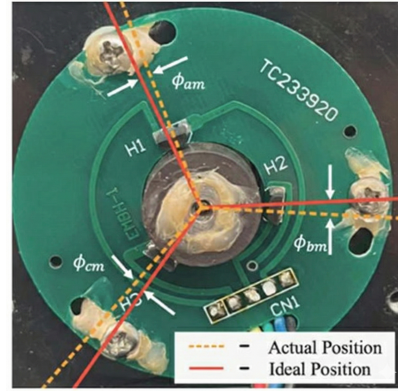


Fig. 3: Manufacturing tolerances in Hall sensor placement lead to misalignment from ideal 120° spacing.

cycle should be equal: $\Delta t_n = T_e/6$, where $T_e = 2\pi/\omega_r$ is the electrical period. However, with Hall misalignment, the intervals become [2]

$$\Delta t_n = \frac{\pi/3 + \Delta\epsilon_n}{\omega_r} \quad (1.11)$$

creating uneven conduction intervals and distort phase currents.

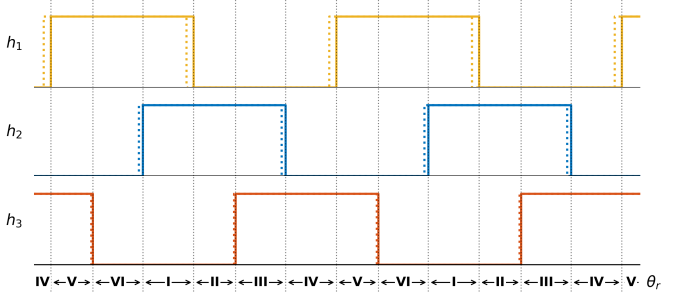


Fig. 4: Hall sensor misalignment causes uneven switching intervals, resulting in distorted phase currents and increased low-frequency torque ripple.

The uneven switching intervals have two detrimental effects on MTPA control. First, the rotor position estimation $\hat{\theta}_r$ used in the Park transformation (1.2) becomes inaccurate. Since the transformation matrix $\mathbf{K}_s^r(\hat{\theta}_r)$ depends directly on the rotor angle, errors in $\hat{\theta}_r$ propagate through to the calculated dq currents in (1.3) and (1.4), introducing oscillations in the measured i_d and i_q .

Second, and more critically for MTPA operation, the time-averaged d -axis current calculation becomes corrupted. The averaging window should ideally span one switching interval of constant duration. However, with misaligned Hall sensors, the intervals Δt_n fluctuate according to (1.11). This causes \bar{i}_d to oscillate even when the motor is in true MTPA condition, making the PI controller respond to measurement artifacts rather than actual d -axis current errors. The result is incorrect

firing angle compensation ϕ_v and potential instability in the MTPA loop.

II. HALL SENSOR SIGNAL CORRECTION VIA LOOKUP TABLE CALIBRATION

Hall sensor misalignment corrupts the switching interval timing, which degrades both steady-state performance and the accuracy of the MTPA controller. This section first reviews conventional averaging filter approaches and their limitations, then presents the proposed Lookup Table (LUT) based calibration strategy that eliminates filter-induced delays while preserving correction accuracy.

A. Limitations of Averaging Filter Approaches

Previous research has proposed moving average filters to smooth the irregular Hall intervals caused by sensor misalignment [1]. These filters operate on the sequence of measured time intervals $\{\Delta t_n\}$ between consecutive Hall transitions and output smoothed values $\{\Delta t'_n\}$ that approximate ideal equal spacing. A typical M -step averaging filter has the form

$$\Delta t'_n = \sum_{m=0}^{M-1} b_m \Delta t_{n-m} \quad (2.1)$$

where the coefficients b_m sum to unity. For example, the 3-step and 6-step extrapolating filters from [1] use correction terms of the form

$$\tau_{a3}^{corr}(n) = \frac{1}{3}(\tau(n-2) + 2\tau(n-3)) \quad (2.2)$$

$$\tau_{a6}^{corr}(n) = \frac{1}{3} \left(-\tau(n-1) + \sum_{k=3}^6 \tau(n-k) \right) \quad (2.3)$$

where $\tau(n)$ denotes the measured time interval for the n -th switching sector.

These filters successfully balance the conduction intervals in steady state by attenuating the harmonics in the interval sequence $\{\Delta t_n\}$. However, the critical drawback is that any averaging filter with memory introduces a delay [1], [2]. During transients such as rapid accelerations or load changes, this delay causes the estimated rotor speed $\hat{\omega}_r$ to lag the actual speed ω_r . The result is a mismatch in the calculated rotor position $\hat{\theta}_r$, which propagates through the Park transformation (1.2) and corrupts the computed d -axis and q -axis currents.

For the MTPA controller, this lag is particularly problematic. The controller relies on an accurate calculation of the average d -axis current \bar{i}_{ds} to determine the required firing angle compensation. When $\hat{\theta}_r$ lags the true position due to filter delay, the measured \bar{i}_{ds} oscillates even when the motor is operating at the true MTPA condition, causing the PI controller to make incorrect adjustments. This can lead to instability in the MTPA loop and degraded transient response, which is unacceptable for applications requiring rapid dynamic performance such as robotics and electric vehicles.

B. Proposed LUT-Based Calibration Strategy

To eliminate the delay caused by memories while preserving correction accuracy, this work employs a two-stage Lookup Table (LUT) based approach [2]. The key idea is that Hall sensor misalignment is a fixed geometric error that does not change during operation. Therefore, the correction values can be identified once during a calibration phase and then applied instantaneously during runtime without any filtering.

For this study, a high-order averaging filter such as the 6-step filter from (2.3) was used. The filter has good steady-state performance in balancing the Hall intervals but has significant delay, thus it does not have a good transient response. As such, it is a good candidate to be compared against the proposed LUT method. The chosen filter is applied to balance the measured Hall intervals and remove the effects of misalignment by outputting the correction time. The filtered interval $\tau'(n)$ represents what the commutation interval duration would be if the Hall sensors were ideally positioned.

For each of the six Hall states $S \in \{1, 2, 3, 4, 5, 6\}$, the filter would learn the specific time duration for each sector at that specific reference speed, $\bar{\tau}[S]|_{\omega=\omega_{ref}}$. Furthermore, we can get a speed estimate $\hat{\omega}_r$ at that operating point using the filtered intervals [6]. Where the speed estimate is computed as

$$\hat{\omega}_r[n] = \frac{\pi/3}{t_{software}^{ISR}[n] - t_{software}^{ISR}[n-1]} \quad (2.4)$$

Where $t_{software}^{ISR}[n]$ is the software timestamp of the current Hall transition and $t_{software}^{ISR}[n-1]$ is the software timestamp of the previous Hall transition.

The misalignment angle in each state can then be calculated with.

$$\Delta\phi_{LUT}[S] = \hat{\omega}_r[n] \cdot \bar{\tau}[S]|_{\omega=\omega_{ref}} \quad (2.5)$$

The angular corrections for all six Hall states are recorded and stored in a Lookup Table. Note that these corrections represent geometric errors in sensor placement, and thus they remain valid across all operating conditions and speeds. The calibration only needs to be performed once after motor assembly or can be repeated if the Hall sensor PCB is replaced. For subsequent operation, the controller can apply these pre-computed corrections during startup and directly without any filtering, eliminating runtime delay as shown in Figure 5.

C. Implementation of LUT Calibration and Operation

The overall control flow is illustrated in Figure 5 which simulates the calibration routine in a microcontroller. The interrupt service routine (ISR) is triggered by a change in Hall states, defined as

$$S = 4H_1 + 2H_2 + H_3 \quad (2.6)$$

The ISR calculates and save the time durations $\tau_{filter}^{corr}(n)$ into the memory by using the correction values from the filter of choice. If the calibration flag is still active, the calculated correction values are also stored into the LUT by using the estimated speed from equation (2.4). The next scheduled time

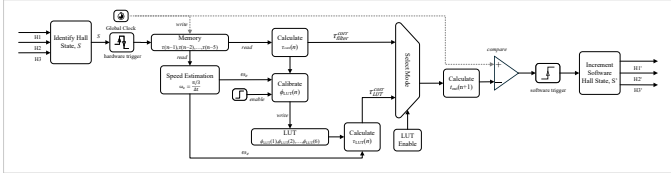


Fig. 5: Control flow diagram showing the transition from calibration mode (using averaging filter to identify errors) to runtime mode (using LUT correction for zero-delay operation).

for advancing the hall state is then determined by adding the corrected interval to the current timestamp,

$$t_{software}^{ISR}(n+1) = t_{hardware}^{ISR}(n) + \tau_{filter}^{corr}(n) \quad (2.7)$$

This software scheduled time is then compared against the hardware timer to trigger the next commutation event. With this algorithm, the Hall intervals are balanced, removing the effects of misalignment. The control then continues to populate the LUT until all six Hall states have been recorded.

After the LUT table is populated, the calibration flag is turned off, and the controller switches to use values from the LUT for calculating the time correction. Hence, the process is similar but now the ISR retrieves the pre-computed correction from the LUT. The calculated correction interval, $\tau_{LUT}^{corr}(n)$, is obtained using (2.5) and the next scheduled time now becomes

$$t_{software}^{ISR}(n+1) = t_{hardware}^{ISR}(n) + \tau_{LUT}^{corr}(n) \quad (2.8)$$

The values for the LUT are also retained in non-volatile memory so that they can be loaded at startup for all subsequent operations without needing to recalibrate.

Since values for time correction are pre-computed and stored in the LUT, this correction approach eliminates the phase lag from filter approach while correcting the Hall sensor misalignment error [2]. The LUT-based method thus preserves the system's dynamic response capability while achieving the same steady-state correction accuracy as high-order averaging filters.

D. Implementation Considerations

The LUT requires minimal memory, storing only six angular correction values (one per Hall state). On a typical microcontroller, this consumes less than 24 bytes. The runtime computation in (??) involves one table lookup, one subtraction, and one division, which can be executed within microseconds on modern DSPs.

The calibration phase can be automated as part of the motor commissioning process. The motor is accelerated to a moderate speed, and correction values are identified over several electrical cycles to ensure statistical reliability. Once calibrated, the LUT values are stored in non-volatile memory and loaded at startup for all subsequent operations.

Another advantage of LUT is that it can be used for more accurate speed estimation. Since we know the angles between each commutation sector, we can use this to get a more accurate speed for each sector.

III. MTPA USING PI CONTROLLER FOR DYNAMIC ADVANCE ANGLE COMPENSATION

With the Hall sensor timing corrected by the LUT-based strategy from Section II, the control system can now implement Maximum Torque per Ampere (MTPA) operation reliably. As discussed in Section I-C, motors with large stator inductance experience phase lag between the phase current and back-EMF. The standard 30° advance angle in COM needs another angle correction term to compensate for this lag,

$$\phi_v' = 30 + \Delta\phi_v \quad (3.1)$$

Since $\Delta\phi_v$ depends on the operating conditions, this section presents a PI-based controller that dynamically adjusts the firing angle to maintain the MTPA condition across varying speed and load.

A. d-Axis Current Regulation for MTPA

Recall from (1.7) that maximum torque per ampere is achieved when $i_d = 0$. Therefore, the control objective for MTPA is to maintain the time-averaged d-axis current at zero: $\bar{i}_d = 0$ [10].

Using the corrected rotor position estimate $\hat{\theta}_r$ from the LUT-based Hall correction, the instantaneous stator currents are transformed into the synchronous reference frame. The d-axis current i_{ds} is extracted via the Park transformation matrix \mathbf{K}_s^r from (1.2):

$$\mathbf{i}_{dqs} = \mathbf{K}_s^r \cdot \mathbf{i}_{abcs} \quad (3.2)$$

The six-step commutation produces discontinuous phase currents, causing $i_{ds}(t)$ to contain high-frequency harmonics. To obtain a stable control signal, $i_{ds}(t)$ is averaged over one electrical cycle [1]:

$$\bar{i}_{ds}[n] = \frac{1}{T} \int_{t_n}^{t_n+T} i_{ds}(t) dt \quad (3.3)$$

where T is the duration of one electrical cycle and t_n is the starting time of the n -th electrical cycle. Then a PI Controller When $\bar{i}_{ds} = 0$, the fundamental component of the phase current is aligned with the back-EMF, achieving MTPA operation [1], [7].

B. PI Controller for Dynamic Angle Compensation

A Proportional-Integral (PI) controller drives \bar{i}_{ds} to zero by compensating the advance firing angle. The control error is simply the negative of the averaged d-axis current:

$$e[n] = -\bar{i}_{ds}[n] \quad (3.4)$$

The PI controller outputs a compensation angle $\Delta\phi_v[n]$:

$$\Delta\phi_v[n] = K_p e[n] + K_i \sum_{j=0}^n e[j] \quad (3.5)$$

where K_p and K_i are the proportional and integral gains. The proportional term provides fast response, while the integral term eliminates steady-state error.

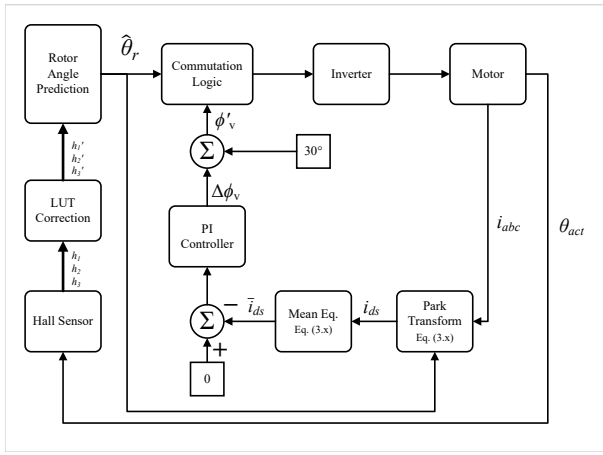


Fig. 6: Flowchart of the MTPA PI controller. The corrected Hall signals provide accurate $\hat{\theta}_r$ for computing i_{ds} from phase currents. The average \bar{i}_{ds} is fed to the PI controller, which outputs compensation angle $\Delta\phi_v$ to maintain MTPA.

The total firing angle combines the COM advance with the dynamic compensation:

$$\phi'_v[n] = 30 + \Delta\phi_v[n] \quad (3.6)$$

This corrected angle ϕ'_v adjusts when the VSI commutes relative to Hall transitions. At higher speeds, the inductive lag increases due to the rotational coupling term $\omega_r L_s i_q$ in (1.4), requiring larger $\Delta\phi_v$. Similarly, at higher torque (larger i_q), the current rise time during commutation is longer, also requiring more advance. By using PI controller, the system can automatically find the optimal $\Delta\phi_v$ for each operating point for MTPA operation.

Together with the LUT-based Hall correction from Section II, this combined control architecture [1] enables BLDC motors with Hall sensor misalignment and large stator inductance to achieve near-optimal MTPA operation. The commutation timing is influenced by both corrections:

$$t_{out}(n) = t_{in}(n) + \tau_{corr}(n) - \frac{\Delta\phi_v[n]}{\hat{\omega}_r[n]} \quad (3.7)$$

where the first correction term $\tau_{corr}(n)$ from (??) balances the Hall intervals, and the second term applies the MTPA advance compensation. The system dynamically adjusts both corrections in real time to maintain optimal performance.

IV. DETAILED MACHINE SIMULATIONS

The proposed combined control strategy was validated using Simulink and a common industrial BLDC motor. The motor parameters are listed in the B.

A. Validation of LUT and MTPA Controller

To validate the effectiveness of the proposed LUT-based Hall correction and MTPA controller, we will compare the method against the model in past literatures [1], [2].

First the motor is simulated with Hall sensor misalignment of $+9^\circ$, -1° , and $+7^\circ$ for H_1 , H_2 , and H_3 respectively. By

running the calibration phase with the 6-step averaging filter from (2.3), the LUT correction angles for each sector can be visualized as shown in Figure 7.

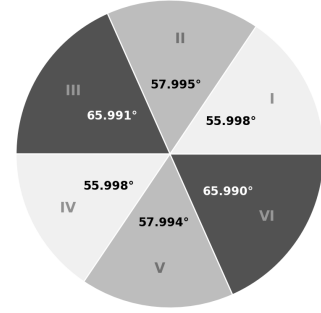


Fig. 7: Visualised LUT correction angles for Hall sensor misalignment.

Then, Figure 8 compares the behaviour of Hall correction either with LUT or filter, along with MTPA. The figure is divided into three sequential stages to illustrate the sequence of operations each controller do. Initially, both methods start with no Hall compensation, resulting in significant oscillations in i_d and \bar{i}_d . Then the Hall correction is enabled either through the filter (a) or LUT (b). Observe that both methods successfully balance the switching intervals as indicated by the symmetric current waveform. Consequently, the oscillations in i_d and \bar{i}_d are eliminated, with \bar{i}_d reaching a non zero constant value. This confirms the validity of using LUT for Hall correction, achieving similar steady-state performance as the filter method in past studies. Figure 8

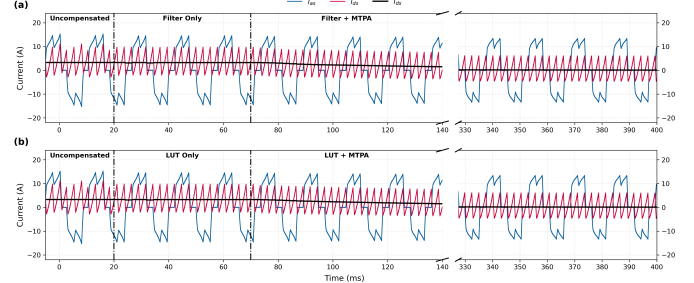


Fig. 8: Simulated phase current i_a , d-axis current i_d , and time averaged d-axis current \bar{i}_d for (a) Filter, (b) MTPA.

Since the \bar{i}_d is now stable, it is now suitable for MTPA control. Note that after the MTPA is activated, the PI controller quickly drives \bar{i}_d to zero, achieving MTPA operation. From Section III we can verify the effectiveness of the MTPA by observing the alignment of phase currents and back-EMF.

Figure 9 compares the uncompensated case (a), the LUT-only case (b), and the combined Method (c). The uncompensated waveforms show significant distortion and phase lag. The filter balances the switching intervals, but the phase lag persists. Finally, combining the LUT with MTPA (c), the controller achieves both balanced intervals and aligns the

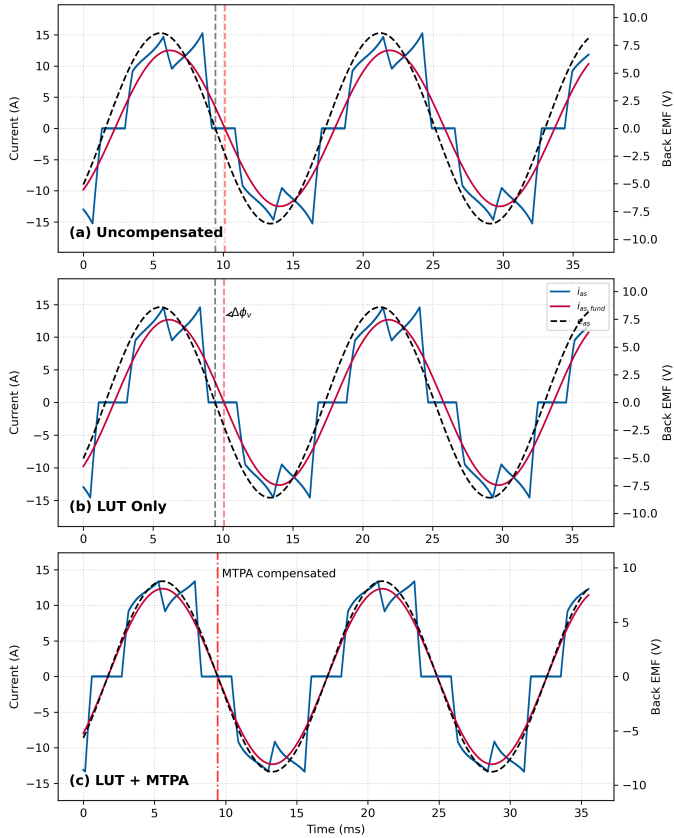


Fig. 9: Alignment of the fundamental phase current and back-EMF: (a) uncompensated; (b) LUT only; (c) LUT + MTPA controller.

fundamental phase current and back-EMF and we achieve MTPA operation.

Figure 10 presents the steady-state performance comparison in terms of torque generation efficiency, defined as the ratio of average torque to RMS phase current ($K_t = \bar{T}_e / I_{rms}$). The uncompensated case exhibits the lowest efficiency due to significant phase misalignment. The filter-only approach improves commutation symmetry but introduces delays that prevent optimal torque production. The proposed combined method (LUT + MTPA) demonstrates the highest torque-per-ampere ratio, confirming that the algorithm successfully compensates for both Hall sensor placement errors and inductive phase lag, thereby recovering the optimal operating point.

B. Transient Performance

Figure 11 illustrates the speed response of the motor when applying the filter from startup. As shown, the proposed LUT correction achieves a response time comparable to the ideal sensor placement and the Hall intervals are corrected from startup. In contrast, the 3-step and 6-step averaging filters due to their memory based nature, was not able to be properly initialized from startup. Filter based approach needs to wait for the motor to reach steady state before they can be activated, whereas LUT approach can be used immediately

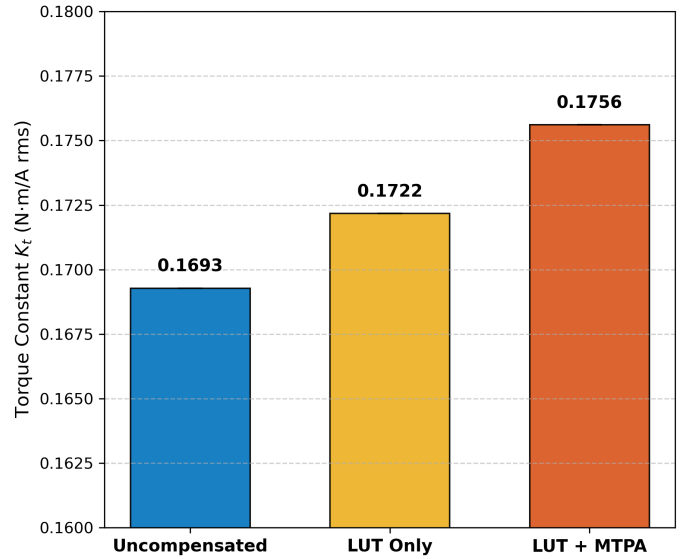


Fig. 10: Comparison of Torque Generation Efficiency (Torque Constant K_t). The proposed LUT + MTPA method achieves the highest torque-per-ampere, indicating optimal alignment.

after the calibration. This demonstrates the advantage of the LUT method in better transient performance.

Figure 12 depicts the system response to a sudden load torque step. The performances are similar.

V. CONCLUSION

This paper presented a unified control framework addressing two critical performance bottlenecks in BLDC drives: sensor misalignment and inductive lag. By integrating a LUT-based calibration with a dynamic MTPA controller, the system achieves smooth and efficient operation. Simulation results confirm the method's ability to eliminate misalignment in Hall sensor signals and achieving maximum torque-per-ampere (MTPA) operation, while maintaining excellent transient response characteristics suitable for dynamic industrial applications. Future research will explore experimental validation through microcontroller implementation.

APPENDIX MOTOR PARAMETERS

The main parameters of the BLDC motor used in this study are listed in Table I.

TABLE I: Motor Parameters

Parameter	Symbol	Value
Stator Resistance	R_s	0.5Ω
Stator Inductance	L_s	1.2 mH
Flux Linkage	ψ_m	0.05 Wb
Pole Pairs	P	4
Rated Speed	ω_{rated}	3000 rpm

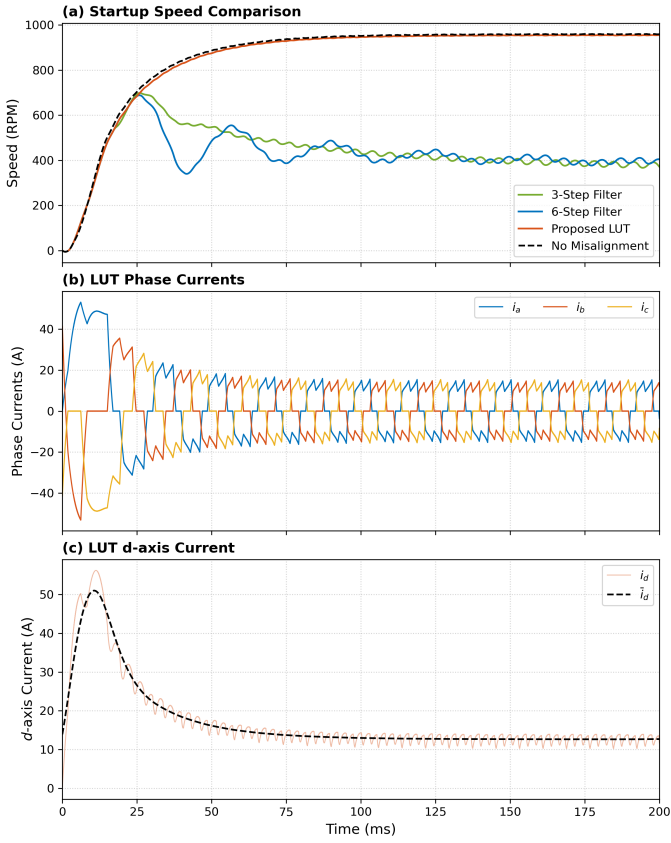


Fig. 11: Simulated speed response step increase. (a) with ideal Hall sensor placement; (b) Comparison of averaging filters vs. proposed LUT correction. The LUT method achieves faster convergence.

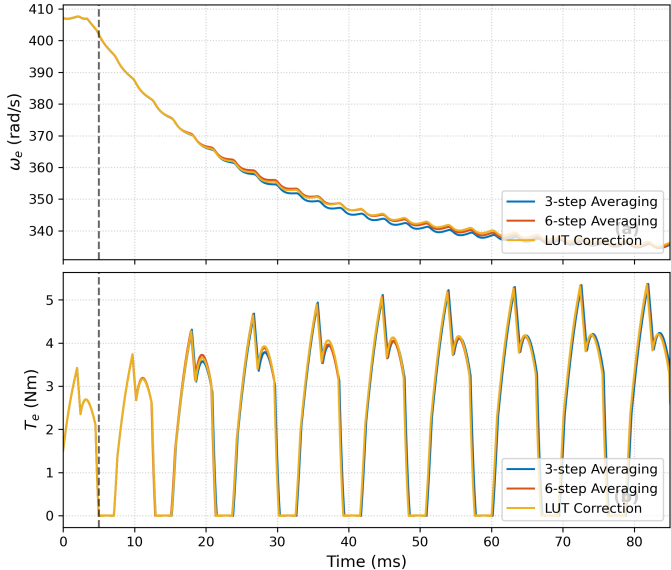


Fig. 12: Simulated response to a load step increase: (a) speed response; (b) electromagnetic torque response. The proposed LUT correction (yellow trace) shows superior dynamic tracking.

APPENDIX PI CONTROLLER GAINS

The PI controller gains used in the MTPA control are listed in Table II.

TABLE II: PI Controller Gains

Gain	Value
Proportional Gain	$K_p = 0.0068$
Integral Gain	$K_i = 0.744$

ACKNOWLEDGMENT

The authors acknowledge the support of the Department of Electrical and Computer Engineering at the University of British Columbia.

REFERENCES

- [1] M. Phung, "Maximum Torque per Ampere Control of Brushless DC Motors with Large Winding Time Constant and Hall-Sensor Misalignment," B.A.Sc. thesis, University of British Columbia, Vancouver, BC, Canada, 2025.
- [2] M. Hasman, "Mitigating Misaligned Hall Sensors in Brushless DC Motors Using a Calibration Routine for Improved Fast Electromechanical Transients," B.A.Sc. thesis, University of British Columbia, Vancouver, BC, Canada, 2025.
- [3] P. C. Krause, O. Wasynczuk, S. D. Pekarek, and T. O'Connell, *Electromechanical Motion Devices: Rotating Magnetic Field-based Analysis with Online Animations*. Hoboken, NJ, USA: Wiley-IEEE Press, 2020.
- [4] P. Pillay and R. Krishnan, "Modeling, simulation, and analysis of permanent-magnet motor drives, part II: The brushless DC motor drive," *IEEE Trans. Ind. Appl.*, vol. 25, no. 2, pp. 265–273, Mar./Apr. 1989.
- [5] S. D. Sudhoff and P. C. Krause, "Operating modes of the brushless DC motor with a 120 degrees inverter," *IEEE Trans. Energy Convers.*, vol. 5, no. 3, pp. 558–564, Sep. 1990.
- [6] N. Samoylenko, Q. Han, and J. Jatskevich, "Dynamic Performance of Brushless DC Motors With Unbalanced Hall Sensors," *IEEE Trans. Energy Convers.*, vol. 23, no. 3, pp. 752–763, Sep. 2008.
- [7] P. Alaeinovin, S. Chiniforoosh, and J. Jatskevich, "Evaluating misalignment of hall sensors in brushless DC motors," in *Proc. IEEE Canada Electr. Power Conf.*, Oct. 2008, pp. 1–6.
- [8] J. Zhou, S. Ebrahimi, and J. Jatskevich, "Extended Operation of Brushless DC Motors Beyond 120° under Maximum Torque Per Ampere Control," *IEEE Trans. Energy Convers.*, vol. 38, no. 2, pp. 1–12, Jun. 2023.
- [9] P. Alaeinovin and J. Jatskevich, "Filtering of Hall-Sensor Signals for Improved Operation of Brushless DC Motors," *IEEE Trans. Energy Convers.*, vol. 27, no. 2, pp. 547–549, Jun. 2012.
- [10] J. Zhou, J. Lu, S. Ebrahimi, and J. Jatskevich, "A Compensation of Commutation Angle in Hall-Sensor-Controlled Brushless DC Motors for Maximum Torque per Ampere Operation," in *Proc. 21st Int. Symp. INFOTEH-JAHORINA*, Mar. 2022, pp.
- [11] B. Tan, X. Wang, D. Zhao, K. Shen, J. Zhao, and X. Ding, "A Lag Angle Compensation Strategy of Phase Current for High-Speed BLDC Motors," *IEEE Access*, vol. 7, pp. 9566–9574, 2019.
- [12] X. Shi, X. Wang, C. Gu, and Z. Deng, "A novel commutation correction method for high-speed PM brushless dc motor," in *Proc. IEEE Appl. Power Electron. Conf. Expo. (APEC)*, Mar. 2017, pp. 1899–1905.
- [13] The MathWorks, Inc., *SimPowerSystems: Model and Simulate Electrical Power Systems User's Guide*. Natick, MA, USA: The MathWorks, Inc., 2006.